Excerpt from the Proceedings of the 2011 COMSOL Conference in Stuttgart

3D FEM Analysis of Micromachined Wind Sensor Based on a Self-heated Thermistor Array

A. Talić[*,1,2], S. Ćerimović[2], M. Mutapčić[2], R. Beigelbeck[1], F. Keplinger[2] and J. Schalko[1,2]
[1]Institute for Integrated Sensor Systems, Austrian Academy of Sciences, Wiener Neustadt, Austria
[2]Institute of Sensor and Actuator Systems, Vienna University of Technology, Vienna, Austria
*Corresponding author: Institute for Integrated Sensor Systems, Viktor Kaplan Str. 2,
A-2700 Wiener Neustadt, Austria, almir.talic@oeaw.ac.at

Abstract: We present COMSOL-based analyses and design optimizations of a micromachined wind sensor. The sensor relies on eight germanium thermistors embedded in a thin silicon nitride membrane, where two orthogonally arranged ensembles, each consisting of four thermistors, are connected to form a double Wheatstone-bridge. In operation, each bridge is supplied by a constant current and the self-heating of the thermistors is utilized as heat source. The developed temperature field depends on direction and magnitude of the fluid flow across the membrane. Evaluating the two bridge voltages facilitates measurement of the flow velocity and direction. The 3D FEM model enables optimized placement and shaping of the thermistors, prediction of the sensor characteristic, and estimation of the excess temperature distribution over the membrane.

Keywords: MEMS, wind sensor, Wheatstone bridge, heat transfer.

1. Introduction

In [1], we presented FEM simulations of a bidirectional micromachined flow sensor featuring a thin silicon nitride membrane where four germanium thermistors are embedded. This sensor can be operated in two different modes. The first mode relies on the calorimetric operation while the second is based on the self-heating of the thermistors combining anemometric and calorimetric transduction principles. This sensor features high sensitivity and very low power consumption [2]. The output signal obtained through a Wheatstone bridge read-out exhibits an approximately sinusoidal characteristic. Combining two orthogonally arranged flow sensors of this type, one for each component of the flow velocity vector, facilitates angular-resolved flow direction measurements. In [3], we reported on a computer mouse operating on this principle. A more convenient way to measure the flow direction is to use a single chip solution where all active elements are embedded on the same membrane. We optimized the sensor structure of such a device by means of extensive 3D FEM modeling. In a first "ad hoc" version, the positions of the thermistors were just copied from the simple (1D) flow sensor design. In further steps, the shape and the position of the thermistors were varied in order to reduce the directional error. This model allows both a detailed study of the sensor characteristic and a calculation of the excess temperature distribution over the membrane.

2. Sensor layout and principle

The proposed wind sensor layout is based on an array of eight germanium thermistors ($R_{\mathrm{th1\text{-}8}}$, Fig. 1a). Two orthogonally arranged ensembles, each consisting of four thermistors, are connected to a double Wheatstone bridge supplied by a constant current I_{SUP} (Fig. 1b). For the thermistor arrangement depicted in Fig. 1 the bridge voltages equals to

$$U_{\mathrm{B,X}} = I_{\mathrm{SUP}} \frac{R_{\mathrm{th1}}R_{\mathrm{th2}} - R_{\mathrm{th3}}R_{\mathrm{th4}}}{R_{\mathrm{th1}} + R_{\mathrm{th2}} + R_{\mathrm{th3}} + R_{\mathrm{th4}}},$$
$$U_{\mathrm{B,Y}} = I_{\mathrm{SUP}} \frac{R_{\mathrm{th5}}R_{\mathrm{th6}} - R_{\mathrm{th7}}R_{\mathrm{th8}}}{R_{\mathrm{th5}} + R_{\mathrm{th6}} + R_{\mathrm{th7}} + R_{\mathrm{th8}}}. \quad (1)$$

The sensor is based on a combined calorimetric-anemometric measurement principle, where the self-heating of the thermistors was utilized as a heat source. At zero flow, the temperature field generated by the thermistors is approximately 4-fold rotational symmetric regarding the membrane midpoint. The inner (R_{th2}, R_{th3}, R_{th6}, and R_{th7}) and the outer thermistors (R_{th1}, R_{th4}, R_{th5}, and R_{th8}) measure the same temperature, respectively. Therefore, the bridges are according to Eq. 1 in balance (i.e., $U_{\mathrm{B,X}} = U_{\mathrm{B,Y}} = 0$).
The convective heat transfer induced by the media flowing across the sensor's surface disturbs the thermal symmetry. In the case of a flow in x-direction (i.e., $\varphi = 0°$ regarding Fig. 1a), the upstream thermistor pair of the first bridge (R_{th1} and R_{th2}) is more cooled down than its downstream counterpart (R_{th3} and R_{th4}). Due to the negative TCR of the thermistors, the difference in the numerator of $U_{\mathrm{B,X}}$ in Eq. 1 increases with increasing flow

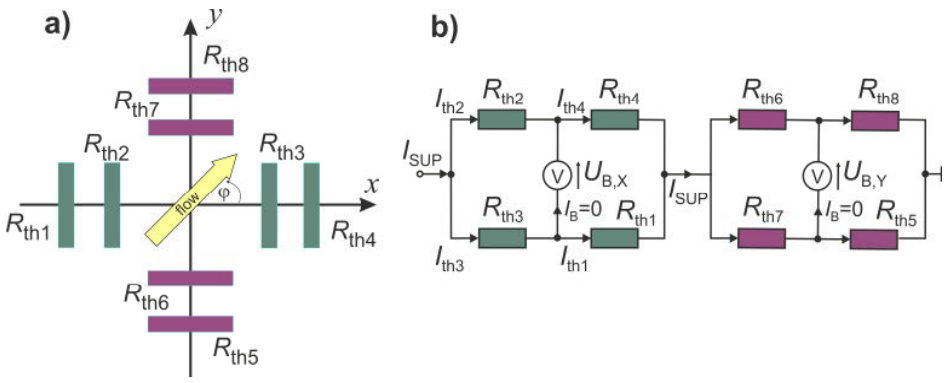

Figure 1. a) Schematic layout of the wind sensor. b) Arrangement of the eight thermistors ($R_{th1\text{-}8}$) in two full bridge configurations.

velocity. On the other hand, the inner thermistors of the second bridge (R_{th6} and R_{th7}) and the outer ones (R_{th5} and R_{th8}) measure the same temperature, respectively. Therefore, $U_{B,Y}$ equals zero for $\varphi = 0°$. Owing to the rotational symmetry as well as the orthogonal arrangement of the thermistor bridges, the directional characteristics of these two outputs are approximately sinusoidal with a 90 degree phase shift between each other. Therefore, the angle of the flow direction with respect to the positive x-direction can be calculated by

$$\varphi = \arctan\left(\frac{U_{B,Y}}{U_{B,X}}\right) \tag{2}$$

whereas the flow velocity is a function of the modulus of the bridge voltages $v = f(|U_B|)$, where

$$|U_B| = \sqrt{U_{B,X}^2 + U_{B,Y}^2}\,. \tag{3}$$

3. Modeling

Figure 2 illustrates a schematic cross section of the model in x-direction. The rectangular sensor membrane (size 1.2 × 1.2 mm²) is suspended by a 350 µm thick bulk silicon frame. The membrane is composed of a SiO_2, Si_3N_4, and SiN_x sandwich structure with an overall thickness of 1.57 µm. For simulations, all three layers are combined to one single layer using averaged thermal properties. The

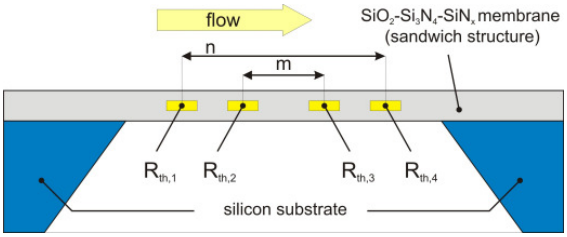

Figure 2. Schematic cross section of the wind sensor in x-direction. The mean distance between inner thermistors is m = 665 µm and outer thermistors n = 935 µm.

heat generating elements are the eight thermistors embedded 0.32 µm above the lower surface of the membrane. A single thermistor measures 400 × 35 µm² exhibiting a total thickness of 0.27 µm.

The applied general heat transfer mode incorporates conduction and convection described by

$$\nabla \cdot (-k\nabla T + \rho C_p T\boldsymbol{u}) = Q, \tag{4}$$

but neglects radiative heat transfer. Here, T, ρ, k, and C_p are the temperature, the density, the thermal conductivity, and the heat capacity of the medium, respectively. Q denotes the density of supplied heat source and $\boldsymbol{u}$ represents the local velocity. Furthermore, the effects of natural convection were not treaded.

Due to the high aspect ratio of the membrane and the embedded thermistors, the number of required mesh elements is rather high. However, it can be significantly reduced by scaling these subdomains with a factor $a = 20$. In order to obtain approximately the same temperature distribution, the material properties must be scaled appropriately according

$$\rho' = \frac{\rho}{a},\ k_x' = \frac{k_x}{a},\ k_y' = \frac{k_y}{a},\ k_z' = k_z a,\ Q' = \frac{Q'}{a}. \tag{5}$$

Here, k_x, k_y, and k_z denote the thermal conductivities in the principal directions of the anisotropic material. In case of thermally isotropic behavior, all three thermal conductivity values are equal, i.e., $k_x = k_y = k_z = k$.

Above the sensor membrane, a rectangular flow channel with h = 1 mm height and w = 2.4 mm width is placed for characterization of the device. The midpoint of the channel's lower side coincides with the midpoint of the membrane surface. The model comprises air domains below (cavity) and above the membrane (in the flow channel) while convective heat transfer is only considered in the latter one. The flow is assumed to be laminar and parallel to the sensor's membrane (i.e., $u_z = 0$). The

imposed flow profile in the channel has the form of a paraboloid

$$\bar{u} = u_{\text{in}} \cdot 1.5 \cdot \left(1 - \left(\frac{z - h/2}{h/2}\right)^2\right) \cdot 1.5 \cdot \left(1 - \left(\frac{r}{w/2}\right)^2\right). \quad (6)$$

$\bar{u}$ is magnitude of the flow velocity, u_{in} is the average flow velocity at flow inlet and r is the shortest distance between the current position (x, y, z) and the plane intersecting the middle of the channel perpendicular to the bottom. This profile implies the required non-slip boundary condition at all flow channel walls. The channel is rotatable such as that any flow direction φ over the full range of 360° can be adjusted (Fig. 1). Thus, r depends on the actual flow direction and can be calculated by the coordinate transformation

$$r = y \cdot \cos(\varphi) - x \cdot \sin(\varphi). \quad (7)$$

With r and $\bar{u}$, the flow velocity components in every point of flow channel equals to

$$u_x = \bar{u} \cdot \cos(\varphi),\ u_y = \bar{u} \cdot \sin(\varphi),\ u_z = 0. \quad (8)$$

The boundary condition at the flow inlet and outlet is implemented as convective flux, the remaining parts of the model circumference were kept at ambient temperature ($T_{\text{amb}} = 20°\text{C}$). This is also the initial temperature value for all domains. The electrical thermistor resistance is modeled as

$$R_{\text{th,i}}(\vartheta) = R_{\text{th,0}} \cdot e^{\alpha \vartheta_i},\ \ \text{i} = 1...8, \quad (9)$$

where $\alpha = -0.02\ /°\text{C}$ is the temperature coefficient of resistivity and $R_{\text{th,0}} = 190\ \text{k}\Omega$ the thermistor resistance at $\vartheta_i = 0°\text{C}$. The thermistor temperatures ϑ_i were calculated through a subdomain integration of the variable T over each thermistor area. The density of the dissipated power in the thermistor reads

$$Q_{\text{i}} = \frac{I_{\text{th,i}}^2 R_{\text{th,i}}(\vartheta_i)}{V},\ \ \text{i} = 1...8, \quad (10)$$

where V specifies the thermistor volume and $I_{\text{th,i}}$ is the thermistor current. It depends indirectly on ϑ_i due to the thermistor effect. The thermistors currents for the first bridge (Fig 1) are expressible by

$$I_{\text{th,1}} = I_{\text{th,3}} = I_{\text{SUP}} \frac{R_{\text{th,2}} + R_{\text{th,4}}}{R_{\text{th,1}} + R_{\text{th,2}} + R_{\text{th,3}} + R_{\text{th,4}}},$$
$$I_{\text{th,2}} = I_{\text{th,4}} = I_{\text{SUP}} \frac{R_{\text{th,1}} + R_{\text{th,3}}}{R_{\text{th,1}} + R_{\text{th,2}} + R_{\text{th,3}} + R_{\text{th,4}}}, \quad (11)$$

where I_{SUP} denotes the bridge supply current. Equivalent expressions can be written for the second bridge. All thermistor temperatures are influenced by convective heat transfer on the one hand and power dissipation Q_{i} on the other hand, which in turn depends on the local temperature (Eq. 10). Starting from the initial temperature, the values $R_{\text{th,i}}$, $I_{\text{th,i}}$, and hence Q_{i} are computed. The first value of Q_{i} is imposed and the thermistor temperatures are calculated anew. In further computational steps, Q_{i} is updated until a steady-state is reached.

4. Simulation results

The simulations were performed assuming an air flow at constant average velocity of $u_{\text{in}} = 1$ m/s and a supply current $I_{\text{SUP}} = 20\ \mu\text{A}$. We utilized the stationary parametric solver varying the flow direction φ in range of 0° to 360° with a 5° increment. After the steady-state of the temperature distribution is reached, the electrical resistance values of the thermistors were acquired. Finally, by applying Eq. 1 the directional characteristics of the bridge voltages were obtained (Fig. 3).

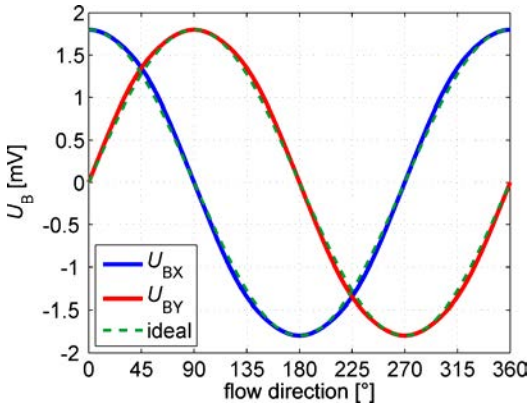

Figure 3. Simulated directional characteristics of the two bridge voltages $U_{\text{B,X}}$ and $U_{\text{B,Y}}$. The hashed lines represent the desired sine and cosine behaviors.

Comparison between simulated values and ideal sine and cosine functions shows significant deviation. To illustrate this more clearly, the value of the angle of the flow direction was determined using the simulated voltages U_{BX} and U_{BY}, applying Eq. 2, and taking into account the sign of the individual voltages to decide the respective quadrant. Figure 4 depicts calculated flow direction versus actual flow direction and the corresponding angle error obtained by the comparison with the ideal characteristic. The maximum angle difference amounts to approximately 2°.

The modulus of the flow direction can be determined by applying Eq. 3 to U_{BX} and U_{BY}. As a constant average flow velocity was imposed, the simulation results in dependence on the flow direction should result in a constant magnitude line. However, the simulated characteristic differs significantly from the constant value (Fig. 5). The

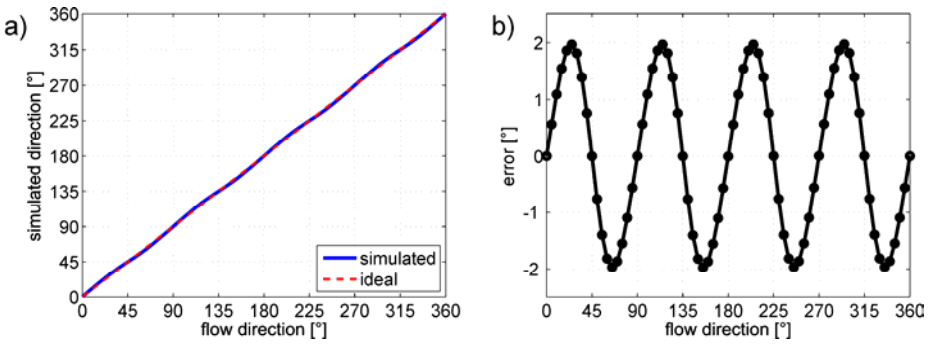

Figure 4. Simulated flow direction (a) and corresponding angle error (b) depending on the actual flow direction for a constant average flow velocity of u_{in} = 1 m/s.

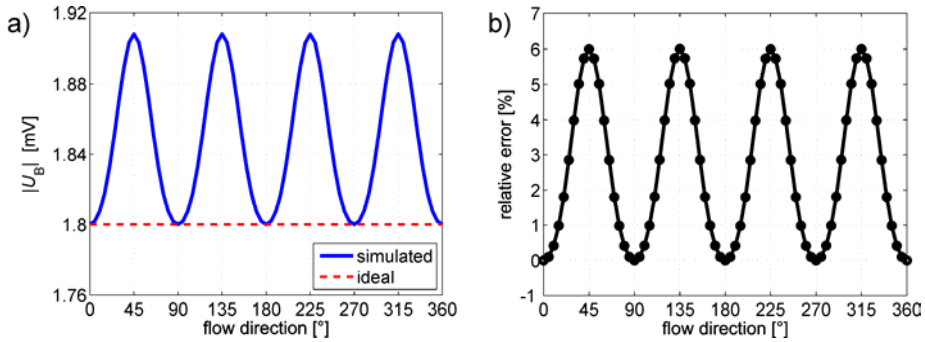

Figure 5. (a) Simulated modulus of the bridge voltages Eq. 3 compared to the reference value as a function of the flow direction at u_{in} = 1 m/s average flow velocity and the corresponding relative error (b).

relative error with respect to the constant reference is strongly dependent on the flow angle and reaches values of up to 6%.

5. Enhanced sensor layout

The simulated angle error (Fig. 4b) and relative error (Fig. 5b) of the "ad hoc" wind sensor version reveals that in the first quadrant the maximum errors occur for $\varphi = 45° \pm 22.5°$. Due to equal shapesize of the thermistors, the large part of the generated heat is bypassed instead to be transferred by the convection to their adjacent, parallel thermistors. This would yield to a reduction of the sensor signal, but at the same time the influence to the adjacent, orthogonal thermistors is maximized. In order to reduce the error, the shape and the dimensions of the thermistors must be changed such that the membrane area covered by the thermistors increases. The presented 3D-FEM model is a convenient tool for this optimization. The best results were achieved with trapezoid-shaped, different-sized thermistors. Figure 6 shows the schematic layout of the enhanced design. The height of both trapezoids is $h = 155$ µm which is more than 4 times the width of the thermistors from the first layout (35 µm). The bottom edge of the smaller thermistors amounts to $a = 100$ µm whereas the upper one is $c = 410$ µm long. The corresponding dimensions of the lager thermistors are $a = 850$ µm and $c = 540$µm. Thus, the total thermistor area is enlarged by more than a factor 5. The mean distance between the inner thermistors (Fig. 2) is now m =505 µm and between outer ones $n = 945$ µm. Due to different geometries, the thermistor resistance at $\vartheta_1 = 0°C$ has to be modified (see Eq. 9). For the inner thermistors the new value is $R_{th,0} = 60$ kΩ whereas for outer thermistors the modified value is $R_{th,0} = 22$ kΩ. The larger area combined with a new shape has a huge impact on the angle and magnitude error.

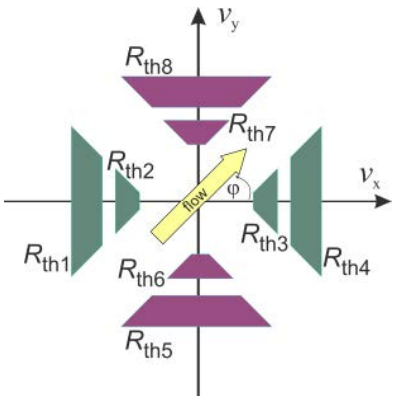

Figure 6. Schematic layout of the enhanced wind sensor. The trapezoid-shaped thermistors increased the thermistor area of the membrane.

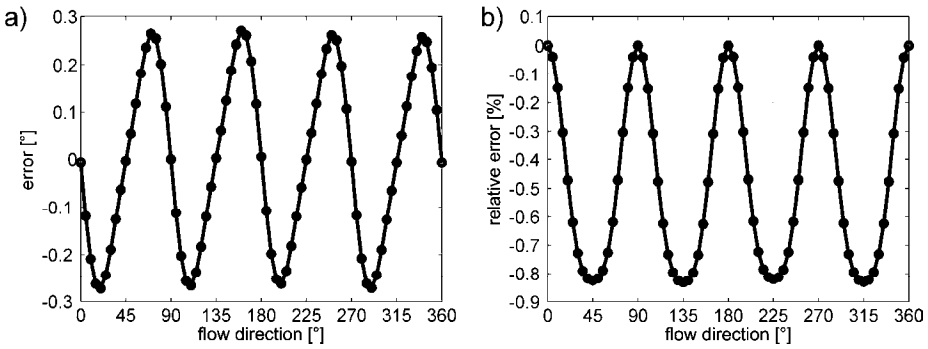

Figure 7. (a) Simulated angle error as well as relative magnitude error (b) for the enhanced sensor layout depending on the flow direction at constant average flow velocity of u_{in} = 1 m/s.

In order to achieve comparable results, all simulation parameters remained unchanged except the supply current was modified to $I_{SUP} = 43$ µm which insures an average dissipated heat power of approximately 0.1 mW for both cases. Figure 7 illustrates the obtained errors. The maximal directional error is below 0.3°, i.e., seven times lower than for the first layout. The relative error of the magnitude is also almost negligible. It amounts to approximately only 0.8%. A further increase of the total thermistor area is not possible owing to the interconnecting leads between bond-pads and membrane elements. In the simplified 3D-Model the interconnection leads were omitted, but they must be accounted for when designing the sensor layout.

Besides the estimation of the output signal and the corresponding transduction errors, the 3D-FEM model is also convenient to predict the maximum over-temperature of the membrane. Figure 8 illustrates the results. For all simulations, only the membrane sector with the diameter equal to the channel width is needed. The rest of the sensor can be omitted yielding a significant reduction of the total number of mesh elements and hence the memory requirements. The highest over-temperature occurs around the inner thermistors. They feature higher dissipated power per unit volume, due to the smaller dimensions and higher nominal resistance. For the total dissipated power of about 0.1 mW, the maximal over-temperature stays below 1°C. However, the magnitude of the output signal is in the mV range which may result in a poor signal-to-noise ratio. For higher output signals, the total heat power must be increased resulting in over-temperatures in the range of few degrees centigrade.

6. Summary and outlook

We performed FEM simulations of micromachined wind sensors for angular-resolved flow measurements. The sensors are based on a Ge-thermistor array embedded in a silicon nitride membrane. Two orthogonally arranged structures are connected to a double Wheatstone bridge assuming a constant supply current. Due to the orthogonal arrangement, the directional characteristic of the two bridge outputs can be well approximated by sinusoidal functions exhibiting 90 degree phase shift. Therefore, the bridge voltages carry the information about the *x*- and *y*-component of the flow velocity enabling the estimation of the flow direction.

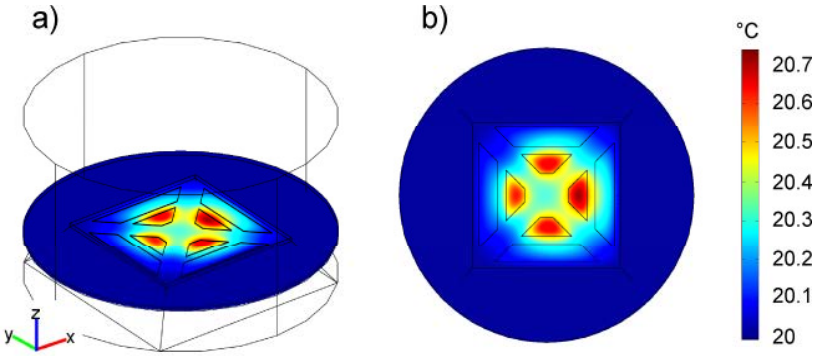

Figure 8. a) 3D-FEM model of the enhanced sensor layout. b) Simulation results for the membrane area obtained for an air average flow velocity of u_{in} = 1 m/s in *x*-direction (φ = 0°). The flow dependent shift of the temperature distribution towards right side is clearly visible.

The first “ad hoc” layout combines the thermistor arrangement of two bidirectional flow sensors. With this simple design, the maximal angular error amounts to 2° and the relative magnitude error to 6%. The new design featuring trapezoid-shaped, non-uniform thermistors enables a reduction of the angle error by a factor of 7 in conjunction with a relative magnitude error below 1%. Moreover, the useful membrane over-temperature is in the range of only few degrees centigrade.

The presented results confirm that the FEM simulations are a convenient method to estimate sensor behavior and its output characteristic. Our next step comprises sensor fabrication and detailed comparison between simulation and measurement results.

7. Acknowledgements

We gratefully acknowledge partial financial support by the Austrian Science Fund FWF (research grants L234-N07 and L657-N16).

8. References

[1] A. Talic, S. Cerimovic, F. Kohl, R. Beigelbeck, F. Keplinger, J. Schalko, "FEM Analysis of Micromachined Flow Sensor with Wheatstone Bridge Read-out", Proceedings of COMSOL Conference, Hannover, Germany (2008).

[2] S. Cerimovic, A. Talic, T. Sauter, F. Kohl, R. Beigelbeck, J. Schalko, A. Jachimowicz:, "A Novel Thermal Transduction Method for sub-mW flow Sensors"; Proceedings of IEEE Sensors, Christchurch, New Zealand, pp 1325-1328 (2009).

[3] S. Cerimovic, M. Forstner, F. Kohl, A. Talic, F. Keplinger, "A Computer Mouse Based on Highly Sensitive Micromachined Flow Sensors", Procedia Engineering, 5, pp 240-243 (2010).